RSC Advances

PAPER

View Article Online
View Journal | View Issue

Cite this: *RSC Adv.*, 2020, **10**, 36546

Preparation of novel morning glory structure γ-MnO_2/carbon nanofiber composite materials with the electrospinning method and their high electrochemical performance

Ziwei Lan,†[a] Lulin Luo,†[a] Jiaye Ye,[a] Qingyue Luo[a] and Lei Zhao *[ab]

Received 25th June 2020
Accepted 14th September 2020

DOI: 10.1039/d0ra05557c

rsc.li/rsc-advances

A novel γ-MnO_2/carbon nanofiber composite electrode material with a morning glory structure was prepared for the first time by electrospinning a mixture solution of $Mn(CH_3COO)_2$ salt and polyacrylonitrile and subsequently treating it with NH_3 atmosphere. The resultant materials were applied in supercapacitors, exhibiting a high voltage of 2 V and high energy density of 15.7 W h kg^{-1} at the current density of 0.5 A g^{-1} in 1 M Na_2SO_4 solution. In this study, precisely controlling the concentration and time of the reaction resulted in the novel morning glory structure. And the morning glory structure at the surface of the carbon nanofibers increased the specific surface area and shortened the diffusion path for charge transport, increasing the Na^+/H^+ ion intercalation capacity, accounting for the high voltage and energy density of the present supercapacitors. These results demonstrated that this new-type of carbon nanofiber with morning glory structure electrode material is potentially superior in obtaining a high voltage for electrode materials and supercapacitors. We hope that these novel materials can expand to different applications in the energy or catalytic field.

Introduction

Supercapacitors, a new energy storage system, are energy storage devices between batteries with faradaic redox and dielectric capacitors and have been arousing more intensive interest for the purpose of protecting the environment.[1,2] Usually, supercapacitors can be divided into two categories according to their energy storage mechanism.[3] One is electrical double-layer capacitors (EDLCs), which involve a non-faradaic redox reaction of pure electrostatic charge accumulation at the electrode–electrolyte interface. The other is pseudocapacitors due to fast and reversible surface redox reactions, which include a metal oxide and conductive polymer involving faradaic redox reactions in the charge/discharge process.[4] In these two categories of supercapacitors, EDLCs use traditional carbonaceous materials (the specific capacitance and energy density are 100–300 F g^{-1} and 5–7 W h kg^{-1}, respectively) as electrode materials, resulting in low energy density, which limits their application.[5] In addition, because of their high electrochemical activity and ability to directly store energy through rapid and reversible redox reactions on the electrode surface, pseudocapacitors with transition metal oxides as an electrode material have been more extensively studied than EDLCs. However, compared to the faradaic process of EDLCs, the non-faradaic process of pseudocapacitors is slow, resulting in low power density and a lack of long-term stability during cycling.[6,7]

Although the energy density of EDLCs using traditional carbon materials as electrode materials is relatively low, carbon materials have always been sought after by researchers due to their high surface area, good electrical conductivity and high electrochemical stability.[8] Recently, it has been reported that researchers have conducted a large number of experimental studies to further realize the application of EDLCs in portable electronic devices, electric vehicles and flexible energy storage systems. Zhou *et al.* obtained MXene-functionalized and cross-linked reduced graphene oxide (rGO) platelets through Ti–O–C covalent bonding, which achieved the bonding of heterogeneous plates between MXene and rGO. As a result, a supercapacitor with super-tough MXene-functionalized graphene sheets realized the dual combination of energy and power density.[9] The interlayer spacing and pore structure of carbon materials are important factors that determine the electrochemical performance of EDLCs. Li *et al.* designed a graphene electrode with high pore utilization rate by tuning the layer spacing of the graphene laminate film. Consequently, the supercapacitor fabricated using this electrode can store capacitance performance compactly and deliver a stack volumetric

[a]*Department of Physical Science and Technology, Lingnan Normal University, Zhanjiang, 524048, China. E-mail: leizhaolingnan@163.com*

[b]*Key Laboratory of Environmentally Friendly Functional Materials and Devices, Lingnan Normal University, Zhanjiang, 524048, China*

† Equal contribution in this paper.

energy density of 88.1 W h L^{-1} in an ionic liquid electrolyte.[9] For the purpose of understanding the energy conversion process of supercapacitors, Krishnamoorthy *et al.* used piezo-electrochemical spectroscopy to probe the energy conversion process of an electrochemical self-charging supercapacitor power cell driven by piezoelectricity. This demonstrated that the self-charging supercapacitor made of siloxene sheets had a self-charging capacity of up to 207 mV under various levels of compressive force.[10] Therefore, tuning the structure of carbon materials and designing high voltage carbon electrodes are the optimum choice for customizing high performance EDLC electrodes.

Among all kinds of pseudocapacitor materials, such as MnO_2, RuO_2, Co_3O_4 and NiO *etc.*, MnO_2 is widely used in supercapacitors because of its excellent theoretical advantages, environmental friendliness, abundant natural storage and simple preparation process.[11] However, MnO_2 materials have poor electrical conductivity, small specific surface area, and easy expansion and shedding during the redox reaction, which has hindered their widespread practical application.[12] Therefore, for practical applications in the future, such as in large energy storage systems, hybrid vehicles, medical equipment, *etc.*,[13] it is imperative to develop supercapacitors with higher working voltages and higher energy. In this way, it is possible to achieve a high cycle life without sacrificing power density under fast charging/discharging to meet the urgent energy needs of people in the present day. According to eqn (1):[14,15]

$$E = \frac{CV^2}{2} \quad (1)$$

the enhancement of the energy density (E) can be achieved by increasing the specific capacitance (C) and/or the working voltage (V) of the supercapacitors. So, the most effective way to obtain higher energy density by increasing the working voltage is to develop a composite electrode material with higher specific capacity, larger specific surface area and higher conductivity, and to widen the working voltage window with a neutral aqueous solution as the electrolyte.

In order to achieve the purpose of high operating voltage and energy density, it is very necessary to combine nanostructured MnO_2 with a highly conductive carbon material to prepare a composite electrode.[16] Through compositing carbon materials, such as activated carbon,[17] carbon nanofibers,[18–20] carbon nanotubes[6,16,21,22] and graphene,[23,24] *etc.*, it is possible to not only shorten the transport path of electrons and reduce the contact resistance, but also provide a larger surface area and increase the number of electroactive sites of electrochemical reaction. Among these carbon materials, carbon nanofibers have attracted much attention due to their unique one-dimensional framework, controllable specific surface area and high conductivity.[25] Simultaneously, the conductivity of electrons can also be further improved by adopting the method of ion doping in the MnO_2-based electrode. Doping atoms (such as Co-doping,[25–27] Ni-doping,[27] N-doping,[28–30] Fe-doping,[27,31] Ce-doping,[32] and Cr-doping,[33] *etc.*) can generate new energy levels and adjust the binding energy of electrons,[25] thereby achieving the purpose of improving the pseudocapacitance and electrocatalytic performance of MnO_2. Recently, many references have combined carbon materials with MnO_2 and doped them with atoms to actualize the effective unification of the EDLC performance and pseudocapacitance. R. Nasser *et al.* synthesized cobalt-doped MnO_2 nanowires modified with graphene oxide by hydrothermal and ultrasonic methods. The analysis results showed that the electrode had a nanocomposite phase structure, and the MnO_2 nanowires had good dispersion on graphene oxide sheets.[26] Li *et al.* prepared a MnO_2/N-APC composite by growing MnO_2 nanosheets on N-doped porous carbon, and the composite exhibited a specific capacitance of 330 F g^{-1} at the current density of 1 A g^{-1}.[28] Li *et al.* synthesized MnO_2 nanosheets doped with transition metals (Fe, Co, Ni, and V) (MONSs) on the internal surface of macroporous carbon (MC), in which the supercapacitor assembled from Ni-doped MONSs had a high specific capacitance of 445 F g^{-1} at the current density of 1 A g^{-1}.[27] Wang *et al.* prepared a Ce-doped MnO_2/rGO composite material by a hydrothermal method. The Ce–MnO_2/rGO composite material was convenient for the quick transport and migration of electrolyte ions during the charge/discharge process, and exhibited good rate capability.[32] Lu *et al.* synthesized a MnO_2/N-doped ultra-microporous carbon nanosphere (MnO_2/N-UCN) composite material by a simple and efficient strategy, which had regular ultramicropores, high surface area, nitrogen heteroatoms, and a high content of MnO_2.[29] Le *et al.* prepared a 3D N-doped graphene/MnO_2 composite material (N-G/MnO_2) using naturally abundant diatomite as a biotemplate, which was used as a bifunctional material for a supercapacitor and oxygen reduction reaction catalyst. Accordingly, the N-G/MnO_2 electrode exhibited a high specific capacitance of 411.5 F g^{-1} at 0.5 A g^{-1} in 1.0 M Na_2SO_4 aqueous electrolyte and achieved a working voltage of up to 1.8 V and 46.1 W h kg^{-1} high energy density.[30] However, there is no characterization study and mechanism analysis of MnO_2/CNF-based supercapacitors using electrospinning technology to prepare biomass carbon material morning glories as conductive skeletons, especially concerning the charging and discharging mechanism of the electrodes.

Herein, for the first time, electrospinning of polyacrylonitrile and $Mn(CH_3COO)_2$ salts was performed to produce carbon and γ-MnO_2 composite materials with a novel morning glory structure, which were used as an electrode material for supercapacitors. The obtained morning glory structure enlarges the cross-section of the carbon nanofibers, and N-doping during the heat treatment of NH_3 improved the conductivity, thus expanding the working potential compared with the conventional carbon nanofibers. In addition, the morning glory structure provided high wettability, conductivity and specific surface area, so as to ameliorate the ion transfer process between the γ-MnO_2/NCNF composites and H^+/Na^+ ions in neutral electrolyte, thus obtaining a high working voltage. The γ-MnO_2/NCNFs-30 composite electrode exhibited a maximum energy density of 15.6 W h kg^{-1} at the current density of 0.5 A g^{-1} in a two-electrode system and the working range in 1 M Na_2SO_4 solution reached 2 V. Furthermore, the electrochemical performance of the electrode materials based on MnO_2 found in this study and other reported works are compared in Table 1,

Table 1 Comparison of the electrochemical performance based on MnO_2 electrode materials

Material	Synthesis	Electrolyte	Specific capacitance/F g^{-1}	Working voltage/V	Stability (cycles)	Ref.
MnO_2	Hydrothermal	1 M Na_2SO_4	197.3 (1 A g^{-1})	1.0	94.6% (1000)	11
MnO_2/AC	Wet impregnation	1 M Na_2SO_4	291 (5 mV s^{-1})	2.0	70% (500)	17
CNFs/MnO_2	Electrospinning	1 M Na_2SO_4	428 (1 A g^{-1})	0.8	98.8% (1500)	20
CNTs/MnO_2	Hydrothermal	1 M Na_2SO_4	405.15 (100 mV s^{-1})	0.8	81% (1000)	22
rGO/MnO_2	Hydrothermal	1 M Na_2SO_4	270 (0.5 A g^{-1})	1.0	90.12% (50 000)	24
Ni-MONSs/MC	Redox reaction	1 M Na_2SO_4	445 (1 A g^{-1})	1.8	93% (1000)	27
Ce–MnO_2/rGO	Hydrothermal	1 M Na_2SO_4	130.44 (1 A g^{-1})	1.0	85% (1000)	32
MnO_2/N-UCNs	Redox reaction	1 M Na_2SO_4	401 (1 A g^{-1})	1.0	86.3% (1000)	29
N-G/MnO_2	Chemical vapor deposition	1 M Na_2SO_4	411.5 (0.5 A g^{-1})	1.8	88.3% (4000)	30
γ-MnO_2/NCNFs	Electrospinning	1 M Na_2SO_4	125 (0.5 A g^{-1})	2.0	92.1% (1000)	This work

which will provide guidance for the development of high-voltage aqueous supercapacitors and allow profound and lasting development of large-scale energy storage devices in the future.

Experimental details

Polyacrylonitrile (PAN), $Mn(CH_3COO)_2$ salt and *N*,*N*-dimethylformamide (DMF) solvent were used for electrospinning. DMF solution was prepared by stirring 3 wt% PAN polymer and 0.9 wt% $Mn(CH_3COO)_2$ (30 wt% compared with PAN) in a magnetic field at 50 °C for 24 hours, to obtain a homogeneously-distributed solution.

The parameters were as follows: the PAN nanofibers were prepared by a conventional electrospinning setup (DW-P503-2ACCD, Dongwen High Voltage Power Supply Company, China), which consists of a high voltage power supply (0–50 kV) and an ordinary hypodermic syringe with a stainless steel needle. During electrospinning the positive terminal (copper wire) of the power supply was connected with the syringe needle and the ground electrode was connected with the collecting substrates. The distance between the needle nozzle and collecting substrates was set at about 15 cm and the electrospinning voltage was 25 kV. Graphitic papers were used to collect the electrospun nanofibers, and no syringe pump was used during electrospinning. The NCNFs were prepared by stabilization and carbonization on the electrospun PAN nanofibers. Stabilization was carried out in air at 250 °C for 2 hours with a heating rate of 5 °C min^{-1}. Carbonization was carried out in an NH_3 atmosphere with a flow rate of 60 mL min^{-1} for 3 hours at 800 °C with a heating rate of 5 °C min^{-1}. Finally, the samples with different amounts of $Mn(CH_3COO)_2$ salt (30 wt%, 60 wt%, and 150 wt% compared with PAN) after NH_3 atmosphere treatment were denoted as MnO_x/NCNFs-30, MnO_x/NCNFs-60 and MnO_x/NCNFs-150.

The structures were characterized by scanning electron microscopy (SEM, Hitachi S-4800), X-ray diffraction (XRD, Rigaku D/max. 2500/PC) and Raman spectroscopy (RM-1000 by Renishaw). A CHI760D (Shanghai Chenhua Instrument Co., Ltd., China) was used for the electrochemical performance test. In the three-electrode electrochemical test, a platinum wire electrode (CHI115) and an Ag/AgCl electrode (CHI111, saturated) were used as the counter electrode and reference electrode, respectively. The mass of electrode material was 1.6 mg and the electrolyte was 1 M Na_2SO_4 solution. The cyclic voltammetry (CV) curves of the three-electrode system were obtained at room temperature in the range of −1 to 1 V at the scan rate of 10–100 mV s^{-1} in 1 M Na_2SO_4 electrolyte. Electrochemical impedance spectroscopy (EIS) measurements were recorded from 10 kHz to 10 MHz with an AC amplitude of 5 mV. Galvanostatic charge/discharge (GCD) measurements were performed at a current density of 0.5, 1, 2, 5 and 10 A g^{-1}.

The specific capacitance can be calculated using eqn (2):[34]

$$C = \frac{I\Delta t}{m\Delta V} \quad (2)$$

and the energy density was estimated by using eqn (1), where C is the capacitance of the three-electrode measuring system or of the two electrodes for the assembled supercapacitors (F g^{-1}), I is the discharge current density (A), m is the mass of the applied active materials of the working electrode for the three-electrode measuring system or the total mass of the active materials of the two electrodes for the assembled supercapacitors (g), ΔV and V are the working potential range for the three-electrode measuring system or working voltage for the assembled supercapacitors (V), Δt stands for the discharging time (s), and E is the energy density (W h kg^{-1}).

Results and discussion

As seen from Fig. 1, the prepared polymer solution was injected into the propulsion device of the electrospinning equipment. Under the action of high DC voltage, a high voltage electric field was formed between the spinning needle and the collecting board, so that the solution was ejected from the spinning needle to generate carbon nanofibers. The generated carbon nanofibers were adsorbed on the collecting board, while Mn^{2+} was regularly attached to the carbon nanofibers. After the prepared carbon nanofibers were subjected to high temperature treatment in an NH_3 atmosphere, NH_3 was decomposed into three active substances (namely H atoms, NH, and NH_2). During the carbonization process, these substances would diffuse to all parts of the internal space of the carbon nanofibers.[35] Then, by combining with their surface atomic bonds, the carbon

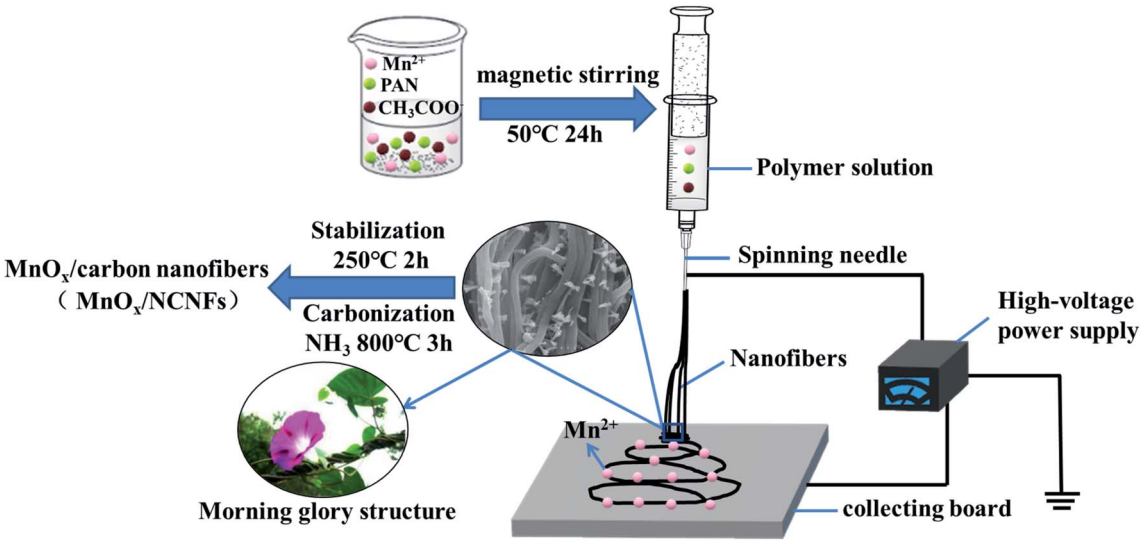

Fig. 1 The flow chart of MnO_x/NCNF preparation by electrospinning.

nanofibers were prevented from agglomerating together to form a large channel with a morning glory structure, so as to stabilize the structure. Meanwhile, Mn^{2+} was oxidized to Mn^{4+} to form MnO_2, and the metal oxide was used as a catalyst to promote the further growth of carbon nanofibers along the radial direction. As mentioned above, the reaction of NH_3 with the active substances in the carbon nanofibers would produce carbon-containing active substances during the gas phase reaction, and the diameter of the carbon nanofibers was reduced under the corrosion of NH_3.[35] Moreover, under the action of the MnO_2 catalyst, these carbon-containing active substances in the form of a carbon source induce the further growth of carbon nanofibers in the radial direction during the chemical phase deposition, thereby promoting the generation of MnO_x/NCNFs.

The carbonization of fibers with different concentrations at 800 °C is shown in Fig. 2. The γ-MnO_2/NCNFs-30 (Fig. 2a–d) shows a morning glory structure, which is more stable and uniform. Correspondingly, MnO_x/NCNFs-60 (Fig. 2e) and MnO_x/NCNFs-150 (Fig. 2f) show a columnar structure, which is not uniform. It can be seen that during the carbonization process, only a fiber shape with too many nodes appeared. The structure of the MnO_x/NCNF composites is a morning glory structure with an average opening diameter of 70 nm and a length of 170 nm growing along the vertical fiber direction. These results can be interpreted as follows: (1) the etching reaction between NH_3 and carbon leads to a reduction in the diameter of NH_3 during the carbonization of nanofibers. (2) At a high temperature of 800 °C, NH_3 decomposes to generate hydrogen atoms or H-containing active species, and immediately reacts with carbon to generate carbon-containing active species or molecules, and thus the diameter of the resulting fibers dwindles. (3) Manganese, as the core catalyst, augments the effective length of H atoms on the surface of the carbon nanofibers in the vertical direction.

The crystallinity and phase composition of the different MnO_x/NCNFs composites were further investigated by XRD as shown in Fig. 3a. All of the observed diffraction peaks can be indexed as graphite, MnO_2 and Mn_3O_4. The 2θ values of the carbon peaks are 26.4°, 44.4°, and 54.5°, corresponding to the (002), (101) and (004) planes of graphite (JCPDS 50-0962).[36] The peaks of MnO_x/NCNFs-30 at 2θ values of 21.9°, 35.2°, 38.4° and 36.8° correspond to the (101), (301), (210), and (111) planes of γ-MnO_2 (JCPDS 42-1316), respectively. Therefore, the prepared MnO_x/NCNFs-30 sample is γ-MnO_2/NCNFs-30.[37,38] However, it can be seen from Fig. 3a that the prepared MnO_x/NCNFs-60 and MnO_x/NCNFs-150 samples are indexed as Mn_3O_4 (JCPDS 75-0962). The Raman spectra of the MnO_x/NCNF composites are shown in Fig. 3b. Two prominent peaks at 1345 and 1588 cm^{-1}

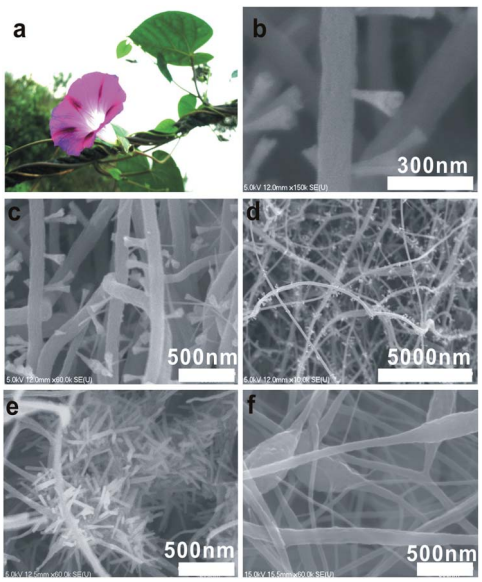

Fig. 2 (a) An image of a morning glory, SEM images of γ-MnO_2/NCNFs-30 at (b) high magnification, (c) medium magnification and (d) low magnification, (e) MnO_x/NCNFs-60 and (f) MnO_x/NCNFs-150.

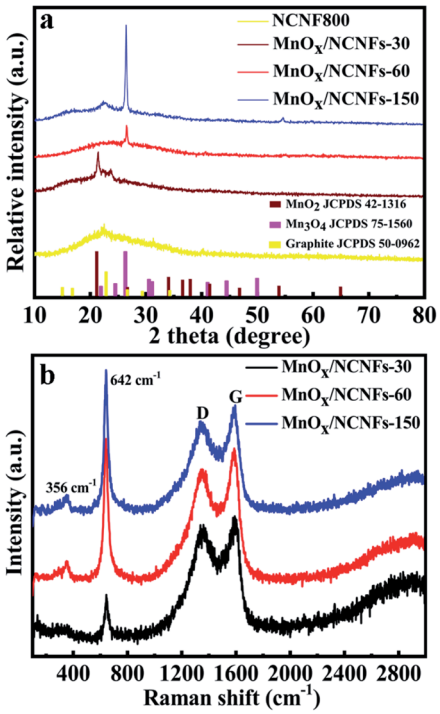

Fig. 3 (a) XRD and (b) Raman patterns of the MnO_x/NCNF composites.

are observed, corresponding to the D and G peaks of the MnO_x/NCNF composites, because N-doping introduces a large amount of topological defects. The G band is caused by doping, defects, stains and other factors, and our results are homogeneous with those of N-doped nanofibers, resulting in the downshift of the G band. Furthermore, the peak value in the range of 500–700 cm^{-1} is deemed to be characteristic of γ-MnO_2, and its specific position is in the range of 630–660 cm^{-1}.[37] What we can see from Fig. 3b is that the most intense peak is located at 645 cm^{-1}, corresponding to the γ-MnO_2 donating the symmetric Mn–O stretching vibration of the MnO_6 group.[39] That of the γ-MnO_2/NCNFs-30 is at 642 cm^{-1}, nearly the same as the value above.[37] The small peaks at 356 cm^{-1} are assigned to the bending modes of Mn–O and the peak at 269 cm^{-1} is a property of γ-MnO_2. The results of the Raman bands for the γ-MnO_2 are in good agreement with the XRD results.

In the three-electrode system, the CV curves of γ-MnO_2/NCNFs-30 are shown at a stable working voltage of 2 V with the scan velocity of 10–100 mV s^{-1} in Fig. 4a. Contrasting with MnO_x/NCNFs-60 and γ-MnO_x/NCNFs-150, γ-MnO_2/NCNFs-30 shows the largest current density in the same potential range. This is because, as compared with the pure carbon nanofiber treated by NH_3 atmosphere, the addition of metal oxides increases the specific capacitance. Furthermore, the addition of manganese salts makes it a catalyst for the growth of carbon materials at 800 °C, which increases the radial growth of the carbon materials and the metallic tendency. As seen from Fig. 2 and 3, γ-MnO_2/NCNFs-30 shows more avenue structures than the other two samples and a γ-MnO_2 structure by contrasting the XRD patterns, which can vastly facilitate the ion charge storage in MnO_2.[40,41] Two mechanisms are based on the surface process and the intercalation/extraction of protons or cations.[42,43] One process is the adsorption/desorption of electrolyte protons or cations, which is often anticipated on the surface of amorphous MnO_2.

$$(MnO_2)_{suface} + M^+ + e^- \leftrightarrow (MnO_2^-M^+)_{surface}$$

The other process is expected to be in crystalline MnO_2.

$$MnO_2 + M^+ \leftrightarrow MnOOM$$

M^+ is Na^+ or H^+ in Na_2SO_4 electrolyte.

The CV curves of γ-MnO_2/NCNFs-30 in the two-electrode system are shown in Fig. 4d, which exhibits a high working voltage. It can be seen that the potential window of the symmetrical supercapacitor assembled with the γ-MnO_2/NCNFs-30 is 0–2 V, and it can work stably at a scanning rate of 0–100 mV s^{-1} at 2 V. Furthermore, the CV curve still maintains the rectangular feature at a high scan rate (100 mV s^{-1}), which demonstrates an outstanding rate capability. Two processes enhance the water decomposition potential, which makes the potential of the γ-MnO_2/NCNFs-30 larger than 1.23 V in 1 M Na_2SO_4 electrolyte. XRD and Raman show that the electrospun MnO_2 is the amorphous structure of γ-MnO_2 as shown in Fig. 5a, which is the irregular alternating growth structure of the pyrolusite (1 × 1) tunnels and ramsdellite (1 × 2) tunnels.[44,45] The structure is incomplete, poorly ordered and defective, but it can compensate for the lack of charge caused by the cation vacancies and low-valence manganese cations through connecting with oxide anions.[44] This study considered that when the potential was lower than the decomposition of water, the nascent hydrogen was absorbed to the surface, resulting in a large specific surface area of the MnO_2 morning glory structure, which immediately interacted into crystalline MnO_2. At fast scan rates, some ions do not have enough time to absorb onto the MnO_2 surface due to the polarization of the hydrated Na^+ ions, and consequently the adsorption on the electrode surface was incomplete. The greatly enhanced ion intercalation capacity is ascribed to the relatively large surface area, ultrastable γ-MnO_2/carbon nanofiber structure and shorter diffusion path for mass and charge transport.[46] Finally, these two reasons above can be fully proved from the redox mechanism diagram of γ-MnO_2/NCNFs-30 in Fig. 5b. As seen from Fig. 5b, the schematic diagram of the redox mechanism of γ-MnO_2/NCNFs-30 can be divided into two parts. In the left part, electrons come in from an external circuit and reduce high-valence ions (Mn^{4+}) to low-valence ions (Mn^{3+}) on the surface and subsurface of the carbon nanofibers, which is a process of rapid reduction of manganese ions.[45,47] In the right part, one process is that the H^+ generated by the decomposition of water and the H^+ in the Na_2SO_4 electrolyte are inserted into the structure of the γ-MnO_2 and react with O^{2-} immediately. The other is that Na^+ in the electrolyte is also inserted into the γ-MnO_2 structure. Eventually, under the action of kinetics, H^+ and Na^+ quickly and uniformly diffuse into the γ-MnO_2 structure. These results

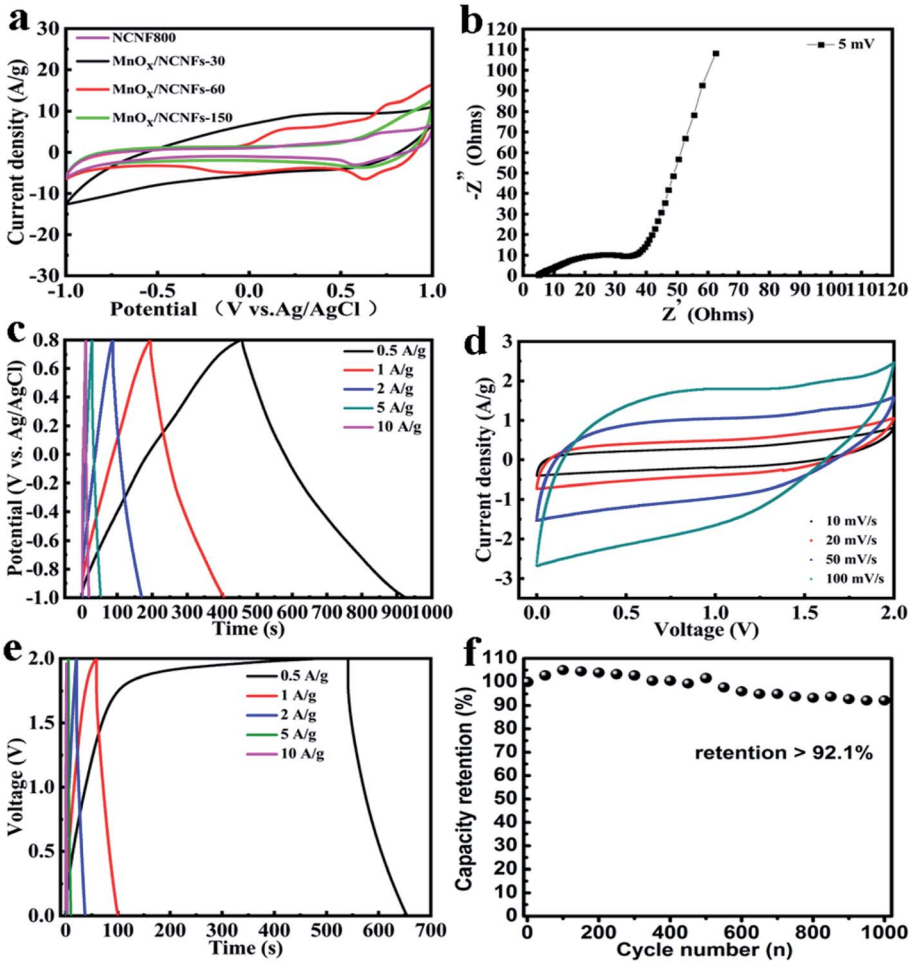

Fig. 4 (a) CV curves of the γ-MnO_2/NCNF composites in a three-electrode system, (b) Nyquist plot of γ-MnO_2/NCNFs-30, (c) charge/discharge curves of γ-MnO_2/NCNFs-30 in a three-electrode system, (d) CV curves of γ-MnO_2/NCNFs-30 in a two-electrode system, (e) charge/discharge curves of γ-MnO_2/NCNFs-30 in a two-electrode system and (f) capacity retention after 1000 cycles.

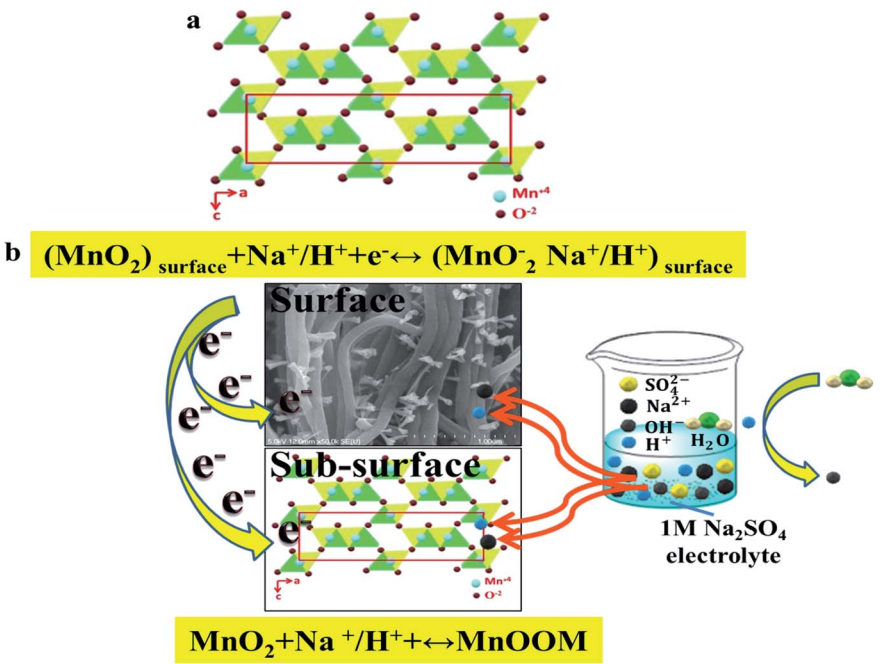

Fig. 5 (a) Crystal structures of γ-MnO_2. (b) Schematic of the γ-MnO_2/NCNFs-30 redox reaction mechanism.

finally indicate that this series of processes enhances the intercalation capacity of Na^+/H^+ ions due to the relatively large surface area, ultra-stable γ-MnO_2/carbon nanofiber structure and shorter diffusion path for charge transport, thereby increasing the working voltage.

From Fig. 4b, the Nyquist plot includes three parts. The high frequency intercept of the semicircle with the real axis represents the internal resistance (R_s),[48] which is 5 ohms. A semicircle in the high-to-medium frequency region is the charge-transfer resistance (R_{ct}).[49,50] It can be seen that R_{ct} (49.7 ohms) is equal to the diameter of the semicircle. The low R_{ct} of γ-MnO_2/NCNFs-30 is due to the morning glory structure, which has a high specific surface area, so that it facilitates the electrolyte cation insertion/extraction process into the nanofiber. In the low frequency region, the Nyquist plot shows a nearly 45° slope relating closely to the middle frequency region (the Warburg impedance),[33] which corresponds to the honeycomb porous nature of the MnO_2 fibers.

The capacitance at the current density of 0.5 A g^{-1} is 125 F g^{-1}, which is shown in Fig. 4c. The variation of the charge/discharge curve with increasing current density not only exhibits symmetry, but also maintains a good specific capacitance. And the initial voltage drop is not obvious with the current density increasing from 0.5 to 10 A g^{-1}, which is attributed to the morning glory structure of the γ-MnO_2/NCNFs-30. The two-electrode system was tested with the total mass of 870 μg (two γ-MnO_2/NCNFs-30 electrodes). It can be calculated that the energy density is 15.6 W h kg^{-1} at the current density of 0.5 A g^{-1} in Fig. 4e. In order to meet the demand of providing high energy density for long cycles at high charge/discharge rates, an excellent electrochemical energy storage device is required. Therefore, the cycling life was investigated over 1000 cycles as shown in Fig. 4f, which showed a stable capacitance retention that remained at 92.1%.

Conclusions

In summary, a new type of γ-MnO_2/carbon nanofiber composite with a morning glory structure was obtained for the first time. It was prepared by electrospinning PAN and $Mn(CH_3COO)_2$ salts, simultaneously, treated by 800 °C thermal treatment under an NH_3 atmosphere. These new-type carbon nanofibers with a morning glory structure not only exhibit an increased specific surface area, but also have an enhanced working potential. The high working voltage of 2 V can be attributed to the following three points. (1) Radial growth can improve the conductivity while improving the wetting performance, and then undergo NH_3 treatment to generate activated functional groups, thereby increasing the forward voltage and expanding the potential window. (2) The material is mainly carbon, because carbon itself is a negative potential material, so the introduction of functional groups can expand the positive potential and increase the working voltage. (3) The large specific surface area of the morning glory structure, ultra-stable γ-MnO_2/carbon nanofiber radial structure and shorter diffusion path for charge transport can enhance the Na^+/H^+ ion intercalation capacity effectively, so as to increase the working voltage. The γ-MnO_2/NCNFs-30 exhibits an energy density of 15.7 W h kg^{-1} at the current density of 0.5 A g^{-1} and a working voltage of 2 V in 1 M Na_2SO_4 electrolyte. The novel structure in this paper not only enriches the family of manganese/carbon composites but also improves the working voltage in the application of supercapacitors.

Conflicts of interest

There are no conflicts to declare.

Acknowledgements

This work was supported by the Science and Technology Program of Zhanjiang government (Grant No. 2019B01002).

Notes and references

1 J. Yan, S. Li, B. Lan, Y. Wu and P. S. Lee, *Adv. Funct. Mater.*, 2020, **30**, 1902564.
2 C. Young, T. Park, J. W. Yi, J. Kim, M. S. A. Hossain, Y. V. Kaneti and Y. Yamauchi, *ChemSusChem*, 2018, **11**, 3546–3558.
3 Q. Zheng, A. Kvit, Z. Cai, Z. Ma and S. Gong, *J. Mater. Chem. A*, 2017, **5**, 12528–12541.
4 A. Xie, F. Tao, C. Jiang, W. Sun, Y. Li, L. Hu, X. Du, S. Luo and C. Yao, *J. Electroanal. Chem.*, 2017, **789**, 29–37.
5 B. Chang, L. Wang, W. Shi, Y. Chai, S. Zhang and B. Yang, *Sustainable Energy Fuels*, 2020, **4**, 2527–2540.
6 L. Li, Z. A. Hu, N. An, Y. Y. Yang, Z. M. Li and H. Y. Wu, *J. Phys. Chem. C*, 2014, **118**, 22865–22872.
7 K. Ghosh, C. Y. Yue, M. M. Sk, R. K. Jena and S. Bi, *Sustainable Energy Fuels*, 2018, **2**, 280–293.
8 S. Korkmaz and İ. A. Kariper, *J. Energy Storage*, 2020, **27**, 101038.
9 T. Zhou, C. Wu, Y. Wang, A. P. Tomsia, M. Li, E. Saiz, S. Fang, R. H. Baughman, L. Jiang and Q. Cheng, *Nat. Commun.*, 2020, **11**, 2077.
10 K. Krishnamoorthy, P. Pazhamalai, V. K. Mariappan, S. S. Nardekar, S. Sahoo and S.-J. Kim, *Nat. Commun.*, 2020, **11**, 2351.
11 S. Zhao, T. Liu, D. Hou, W. Zeng, B. Miao, S. Hussain, X. Peng and M. S. Javed, *Appl. Surf. Sci.*, 2015, **356**, 259–265.
12 J. Ju, H. Zhao, W. Kang, N. Tian, N. Deng and B. Cheng, *Electrochim. Acta*, 2017, **258**, 116–123.
13 Z. Wu, L. Li, J. Yan and X. Zhang, *Adv. Sci.*, 2017, **4**, 1600382.
14 Z. Fan, J. Yan, W. Tong, L. Zhi, G. Ning, T. Li and W. Fei, *Adv. Funct. Mater.*, 2011, **21**, 2366–2375.
15 N. Swain, A. Mitra, B. Saravanakumar, S. K. Balasingam, S. Mohanty, S. K. Nayak and A. Ramadoss, *Electrochim. Acta*, 2020, **342**, 136041.
16 H. Wu, M. La, J. Li, Y. Han, Y. Feng, Q. Peng and C. Hao, *Compos. Interfaces*, 2019, **26**, 659–677.
17 D. Deng, B. Kim, M. Gopiraman and I. S. Kim, *RSC Adv.*, 2015, **5**, 81492–81498.
18 J. H. Jeong, Y. A. Kim and B.-H. Kim, *Carbon*, 2020, **164**, 296–304.

19 J.-G. Wang, Y. Yang, Z.-H. Huang and F. Kang, *J. Power Sources*, 2013, **224**, 86–92.
20 H. Zhao, W. Han, W. Lan, J. Zhou, Z. Zhang, W. Fu and E. Xie, *Electrochim. Acta*, 2016, **222**, 1931–1939.
21 S. Ramesh, H. S. Kim, Y. Haldorai, Y.-K. Han and J.-H. Kim, *Mater. Lett.*, 2017, **196**, 132–136.
22 W. Li, M. Chang, K. Chuang, Y. Li, J. Luo and H. Cheng, *J. Electrochem. Soc.*, 2019, **166**, A2194–A2198.
23 X. Meng, L. Lu and C. Sun, *ACS Appl. Mater. Interfaces*, 2018, **10**, 16474–16481.
24 X. Wang, L. Chen, S. Zhang, X. Chen, Y. Li, J. Liu, F. Lu and Y. Tang, *Colloids Surf., A*, 2019, **573**, 57–66.
25 X. Yang, W. Peng, K. Fu, L. Mao, J. Jin, S. Yang and G. Li, *Electrochim. Acta*, 2020, **340**, 135989.
26 R. Nasser, G.-F. Zhang and J.-M. Song, *Electrochim. Acta*, 2020, **345**, 136198.
27 J. Li, Y. Ren, S. Wang, Z. Ren and J. Yu, *Appl. Mater. Today*, 2016, **3**, 63–72.
28 D. Li, J. Lin, Y. Lu, Y. Huang and C. Tang, *J. Alloys Compd.*, 2019, **815**, 152344.
29 W.-J. Lu, S.-Z. Huang, L. Miao, M.-X. Liu, D.-Z. Zhu, L.-C. Li, H. Duan, Z.-J. Xu and L.-H. Gan, *Chin. Chem. Lett.*, 2017, **28**, 1324–1329.
30 Q. J. Le, M. Huang, T. Wang, X. Y. Liu, L. Sun, X. L. Guo, D. B. Jiang, J. Wang, F. Dong and Y. X. Zhang, *J. Colloid Interface Sci.*, 2019, **544**, 155–163.
31 Z. Wang, F. Wang, Y. Li, J. Hu and M. Xu, *Nanoscale*, 2016, **8**, 7309–7317.
32 Y. Wang, Y. Zhan, X. Yan and Z. Ma, *Russ. J. Electrochem.*, 2018, **54**, 283–291.
33 S. Zhao, T. Liu, Z. Yu, Z. Wen, T. Li, S. Hussain, D. Hou and X. Peng, *J. Mater. Sci.: Mater. Electron.*, 2016, **27**, 3265–3270.
34 L. Zhang, X. Peng, J. Wan, Q. Cui, X. Chu, H. Suo, C. Zhao and D. He, *Nano*, 2020, **15**, 2050031.
35 L. Zhao, Y. Qiu, J. Yu, X. Deng, C. Dai and X. Bai, *Nanoscale*, 2013, **5**, 4902.
36 A. Gomez-Martin, A. Gutierrez-Pardo, J. Martinez-Fernandez and J. Ramirez-Rico, *Fuel Process. Technol.*, 2020, **199**, 106279.
37 C. Julien, M. Massot, S. Rangan, M. Lemal and D. Guyomard, *J. Raman Spectrosc.*, 2002, **33**, 223–228.
38 Y. Chabre and J. Pannetier, *Prog. Solid State Chem.*, 1995, **23**, 1–130.
39 L. Balan, C. M. Ghimbeu, L. Vidal and C. Vixguterl, *Green Chem.*, 2013, **15**, 2191–2199.
40 W. Wei, X. Cui, W. Chen and D. G. Ivey, *Chem. Soc. Rev.*, 2011, **40**, 1697–1721.
41 M. Toupin, T. Brousse and D. Bélanger, *Chem. Mater.*, 2004, **16**, 3184–3190.
42 L. Zhao, J. Yu, W. Li, S. Wang, C. Dai, J. Wu, X. Bai and C. Zhi, *Nano Energy*, 2014, **4**, 39–48.
43 M. Toupin, T. Brousse and D. Bélanger, *Chem. Mater.*, 2002, **14**, 3946–3952.
44 M. I. Said, A. H. Rageh and F. A. Abdel-aal, *RSC Adv.*, 2018, **8**, 18698–18713.
45 J. Arnott, R. Williams, A. Pandolfo and S. Donne, *J. Power Sources*, 2007, **165**, 581–590.
46 X. Duan, J. Yang, H. Gao, J. Ma, L. Jiao and W. Zheng, *CrystEngComm*, 2012, **14**, 4196–4204.
47 Z. Hong and C. Zhenhai, *J. Electrochem. Soc.*, 1989, **136**, 2771.
48 S. Hassan, M. Suzuki and A. A. El-Moneim, *Am. J. Mater. Sci.*, 2012, **2**, 11–14.
49 Z.-H. Huang, Y. Song, D.-Y. Feng, Z. Sun, X. Sun and X.-X. Liu, *ACS Nano*, 2018, **12**, 3557–3567.
50 J. Kavil, P. M. Anjana, P. Periyat and R. B. Rakhi, *Sustainable Energy Fuels*, 2018, **2**, 2244–2251.